The Art of UHF RFID Antenna Design: Impedance-Matching and Size-Reduction Techniques

Gaetano Marrocco

Dipartimento di Informatica Sistemi e Produzione, University of Roma "Tor Vergata"
Via del Politecnico, 1, 00133, Roma, Italy
Tel:+39 06 72597418, Fax:+39 06 72597460; E-mail: marrocco@disp.uniroma2.it

Abstract

Radio-frequency identification technology, based on the reader/tag paradigm, is quickly permeating several aspects of everyday life. The electromagnetic research mainly concerns the design of tag antennas having high efficiency and small size, and suited to complex impedance matching to the embedded electronics. Starting from the available but fragmented open literature, this paper presents a homogeneous survey of relevant methodologies for the design of UHF passive tag antennas. Particular care is taken to illustrate, within a common framework, the basic concepts of the most-used design layouts. The design techniques are illustrated by means of many noncommercial examples.

Keywords: Antennas; RFID; tag; impedance matching; T-match; meander line antenna; small antenna; PIFA; IFA

1. Introduction

The idea of radio-frequency identification (RFID) of objects and remote control of devices was first introduced in late 1948 by H. Stockman [1]. After the big efforts produced by the development of microelectronic technology in the 1970s [2], and the continuing evolution of the last decade [3, 4], RFID is now becoming a pervasive technology [5, 6] in everyday life [7]. It is also being used in more advanced applications, involving logistics, inventory management, systems for disabled people, homeland and personal security, distributed sensor networks [8], and mobile healthcare [9]. A basic RFID system comprises a radio-scanner unit, called a *reader*, and a set of remote transponders, denoted as *tags*. The tags include an antenna and a microchip transmitter with internal read/write memory. In passive tags, the energy required to drive the microchip comes from the interrogation system itself. A backscattering modulation is achieved when the microchip acts as a switch, to match or mismatch its internal load to the antenna.

Several frequency bands have been standardized for this technology. Low-frequency (LF, 125-134 kHz) and high-frequency (HF, 13.56 MHz) systems are the most mature and worldwide diffused technology. They are based on quasi-static magnetic flux coupling among the reader's and tag's coils. Ultra-high-frequency (UHF, 860-860 MHz) and microwave (2.4 GHz and 5.8 GHz) systems instead involve electromagnetic interaction among true antennas and permit longer communication links, and they are the emerging technology.

Together with the power sensitivity of the microchip, the tag's antenna plays a key role in the overall RFID system performance factors, such as the overall size, the reading range, and the compatibility with tagged objects. Most of the antennas for UHF omnidirectional tags are commonly fabricated as modified printed dipoles. The design goal is to achieve the inductive input reactance required for the microchip conjugate impedance matching, and to miniaturize the antenna shape. Several tricks are used, and the resulting tags sometimes exhibit charming and nearly artistic layouts.

Although many tag configurations can be retrieved in scientific papers, or even in the catalogs of commercial products, there is a lack of systematization of the design methodology. A first tutorial paper was available in [10], where the concept of conjugate impedance matching to the microchip was reviewed, some performance parameters were introduced, and fabrication and measurement procedures were described in some detail.

This paper provides a unitary and general survey of the most-used design procedures for miniaturized tag antennas with a complex impedance matched to the microchip load. Attention is devoted to the rationale and to the main features of basic configurations, by the modification and combination of which a great variety of tag layouts can be easily obtained. For each design solution, the role of the main geometrical parameters over the complex impedance tuning are investigated here by introducing *matching charts*, which are a useful tool to get the same antenna configuration to suit different kinds of microchips.

The rest of this paper is organized into four main sections. Section 2 introduces several techniques for achieving complex impedance matching, such as the T-mach, the proximity-loop, and the nested-slot layouts. Miniaturization and bandwidth issues are addressed in Section 3, with references to meandered and inverted-

 ISSN 1045-9243/2008/$25 ©2008 IEEE

Authorized licensed use limited to: Intel Corporation via the Intel Library. Downloaded on December 6, 2009 at 18:28 from IEEE Xplore. Restrictions apply.

F solutions, corroborated by many examples. Other miscellaneous design issues are addressed in Section 4 and, finally, some measurement and test procedures for UHF tags are presented in Section 5.

2. Methods for Conjugate Impedance Matching

Let the effective power ($EIRP_R$) transmitted by the reader and the sensitivity (P_{chip}) of the tag's transponder, e.g., the RF power required by the microchip electronics to turn on and to perform back-scattering modulation, be fixed. Under the hypothesis of polarization matching between the reader and tag antennas, the maximum activation distance of the tag along the (θ,ϕ) direction [10] is then given by

$$d_{max}(\theta,\phi)=\frac{c}{4\pi f}\sqrt{\frac{EIRP_R}{P_{chip}}\tau G_{tag}(\theta,\phi)}, \qquad (1)$$

where $G_{tag}(\theta,\phi)$ is the tag gain. The factor

$$\tau=\frac{4R_{chip}R_A}{\left|Z_{chip}+Z_A\right|^2}\le 1 \qquad (2)$$

is the *power transmission coefficient*, which accounts for the impedance mismatch between the antenna ($Z_A=R_A+jX_A$) and the microchip ($Z_{chip}=R_{chip}+jX_{chip}$). The microchip impedance depends on the input power, and, since the transponder includes an energy-storage stage, its input reactance is strongly capacitive. Most of the available RFID ASICS (application-specific integrated circuits) in the UHF band exhibit an input reactance roughly ranging from $-100\,\Omega$ to $-400\,\Omega$ [11-13], while the real part is about an order-of-magnitude smaller, or less. The antenna impedance should be inductive in order to achieve conjugate matching, and a large impedance phase angle, $\arctan(Z_A)>45°$, needs to be obtained. Beyond d_{max}, the power collected by the tag decreases below the microchip sensitivity, and the tag becomes unreachable.

To obtain low-cost devices, it is not feasible to use external matching networks involving lumped components. Therefore, the matching mechanisms have to be embedded within the tag's antenna layout.

Several feeding strategies can be adopted for antenna tuning. Those most used are modified versions of the well-known T-match, proximity coupling to a small loop, and the inclusion of shaped slots. Useful configurations should permit a nearly independent tuning of resistance and reactance when acting on the tag's geometrical parameters.

Some matching techniques will be now reviewed and compared. For clarity, the antenna maximum size is fixed at half a wavelength without giving consideration to the overall size, which could be eventually impracticable for real applications. The miniaturization issues are deferred to the next section. The matching capabilities of the feeding schemes considered will be summarized through impedance charts, where the input resistance and reactance are related to the variation of relevant geometrical parameters. Such a matching scheme is more agile, as the iso-lines for resistance and reactance are mutually parallel. The basic matching schemes are illustrated with the help of some non-commercial examples, taken from the recent open scientific literature.

2.1 T-Match

With reference to Figure 1, the input impedance of a (planar) dipole of length l can be changed by introducing a centered short-circuit stub, as explained in detail in the old book [14], and more recently in [15]. The antenna source is connected to a second dipole of length $a\le l$, placed at a close distance, b, from the first and larger dipole. The electric current distributes along the two main radiators according to the size of their transverse sections. It can be proved [14, 15] that the impedance at the source point is given by

$$Z_{in}=\frac{2Z_t(1+\alpha)^2Z_A}{2Z_t+(1+\alpha)^2Z_A}, \qquad (3)$$

where $Z_t=jZ_0\tan ka/2$ is the input impedance of the short-circuit stub formed by the T-match conductors and part of the dipole; $Z_0\cong 276\log_{10}\left(b/\sqrt{r_e r_e'}\right)$ is the characteristic impedance of the two-conductor transmission line with spacing b; Z_A is the dipole impedance taken at its center in the absence of the T-match connection; $r_e=0.25w$ and $r_e'=8.25w'$ are the equivalent radii of the dipole and of the matching stub, supposed to be planar traces; and $\alpha=\ln(b/r_e')/\ln(b/r_e)$ is the current division factor between the two conductors.

The geometrical parameters, a, b, and the trace's width, w', can be adjusted to match the complex chip impedance, Z_{chip}. The

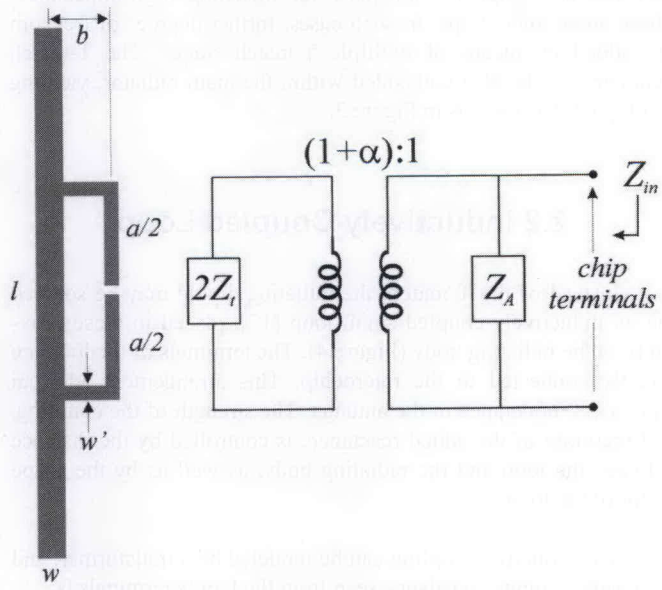

Figure 1. The T-match configuration for planar dipoles and the equivalent circuit, where the impedance step-up ratio $(1+\alpha)$ is related to the conductors' cross sections.

Authorized licensed use limited to: Intel Corporation via the Intel Library. Downloaded on December 6, 2009 at 18:28 from IEEE Xplore. Restrictions apply.

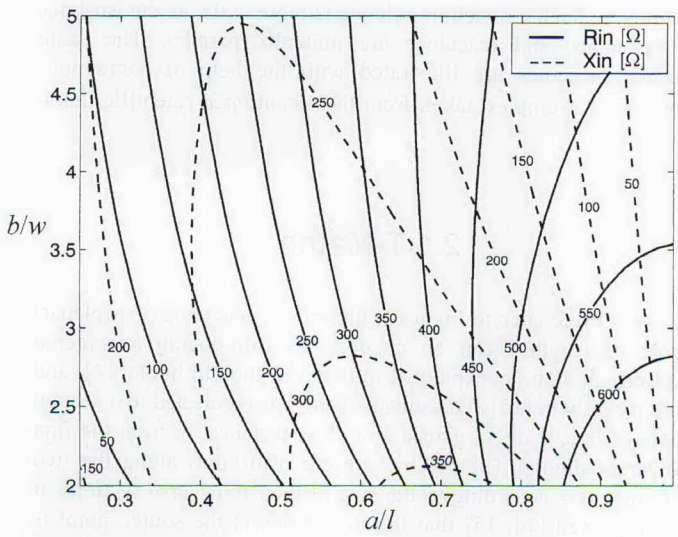

Figure 2. The matching chart for the T-match in Figure 1, for the case of $l = \lambda/2$, $w = \lambda/100$, $w' = w/3$, and $Z_A = 75\,\Omega$.

T-match acts as an impedance transformer (Figure 1). For the case of half-wavelength dipoles, the resulting input impedance at the T-match port is inductive, while for smaller dipoles, the total input impedance can be both capacitive and inductive. For example, Figure 2 shows a matching chart for the T-match layout, with the ratio between the dipoles' cross sections having been fixed to $w/w' = 3$. The input resistance and inductance depend on both the stub sizes a and b, but with different rules. It is known that the cross section of the second conductor has a considerable effect on the resulting antenna impedance. In particular, it can be easily verified from Equation (3) that the increase of the w/w' ratio will raise the impedance values, and the iso-lines for resistance and reactance become nearly vertical and mutually parallel (strongly dependent on the size of b), resulting in a reduced matching agility. Even with small values of a and b, high values of input resistance are generally found. This makes it difficult to match the impedance to real microchip transmitters, unless some shape modification of the main radiator is considered. A single T-match layout could therefore not be completely adequate for matching high-impedance-phase-angle microchips. In such cases, further degrees of freedom are added by means of multiple T-match stages. The T-match geometry can be also embedded within the main radiator, yielding a compact structure, as in Figure 3.

2.2 Inductively Coupled Loop

Instead of the T-match, the radiating dipole may be sourced via an inductively coupled small loop [17], placed in close proximity to the radiating body (Figure 4). The terminals of the loop are directly connected to the microchip. This arrangement adds an equivalent inductance in the antenna. The strength of the coupling, and therefore of the added reactance, is controlled by the distance between the loop and the radiating body, as well as by the shape factor of the loop.

The inductive coupling can be modeled by a transformer, and the resulting input impedance seen from the loop's terminals is

$$Z_{in} = Z_{loop} + \frac{(2\pi f M)^2}{Z_A}, \tag{4}$$

where $Z_{loop} = j2\pi f L_{loop}$ is the loop's input impedance. Whether or not the dipole is at resonance, the total input reactance depends only on the loop inductance, L_{loop}, while the resistance is related to the sole transformer mutual inductance, M:

$$R_{in}(f_0) = (2\pi f_0 M)^2 / R_A(f_0),$$
$$X_{in}(f_0) = 2\pi f_0 L_{loop}. \tag{5}$$

Under the assumption that the radiating body is infinitely long, the loop's inductance and mutual coupling, M, can be expressed in terms of the loop's size and its distance from the dipole through analytical formulas [18]. It is important to note that the mutual coupling, and therefore the total input resistance, are dependent on both the loop's shape and on the dipole-loop distance, while the reactance, L_{loop}, is mainly affected only by the loop's aspect ratio.

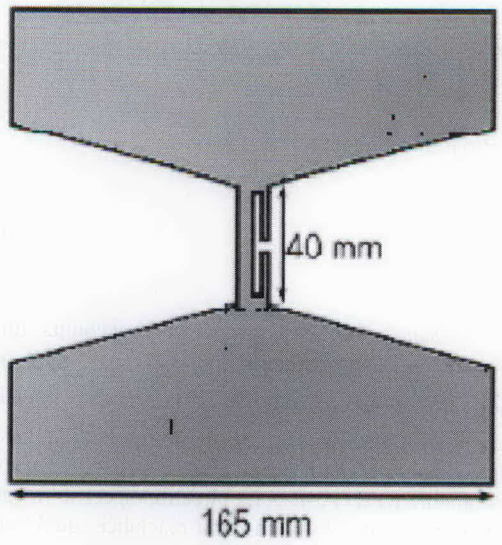

Figure 3. An example of an embedded T-match feed. This antenna was proposed in [16], to be rolled around cardboard reels.

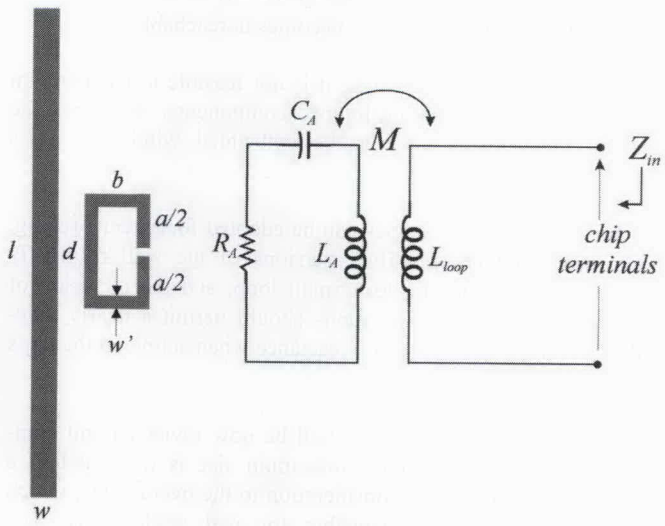

Figure 4. The layout of the inductively coupled feed and its equivalent circuit. The parameters R_A, C_A, and L_A give the circuit model of the radiating body near its (series) resonance.

Authorized licensed use limited to: Intel Corporation via the Intel Library. Downloaded on December 6, 2009 at 18:28 from IEEE Xplore. Restrictions apply.

Figure 5 shows an example of the matching chart, computed by the Method of Moments [19], for the loop-driven dipole, for the particular case of a resonant dipole and a square loop ($a = b$). As expected from Equation (3), the input reactance is nearly unaffected by the loop-dipole distance (d), and the corresponding isolines are vertical. For a fixed loop size, the resistance reduces when the loop-dipole distance increases. A design procedure could therefore initially select the loop size with the purpose of canceling the chip's capacitive reactance. Further on, a proper loop-dipole distance, d, could be chosen to match the chip's resistance. This layout is particularly effective for microchips having high impedance-phase angle.

2.3 Nested Slot

A completely different matching strategy, useful for tags fabricated with large planar dipoles or suspended patches [20, 21], may employ a nested, shaped slot (Figure 6a). Thanks to the inductive reactance of a nonresonant slot, this feeding strategy has the relevant capability of complex impedance matching, even when the tag is attached onto a high-permittivity substrate (see, for instance, Figure 6b). The slot profile can be seen as a slot-line impedance transformer, where each discontinuity (tooth) provides energy storage and radiation. By increasing the number of teeth, further degrees of freedom are added, with the possibility of improving miniaturization and achieving multi-band features [22]. Since the slot sizes may be comparable to the patch surface, the radiation features are related to both objects. In particular, the maximum antenna gain is fixed mainly by the patch side, l, while the impedance tuning can be changed by acting on the slot's aspect ratio, dimensions a and b. Depending on the shape and on the size of the internal slot, the antenna acts mainly either as an H slot, a broadband dipole, or as a doubly folded dipole. When the slot width, b, is much smaller than the external side, l, a typical RLC behavior can be observed, with strong reactance peaks. As the size b increases, the resonance moves towards dc, and the reactance peak is reduced.

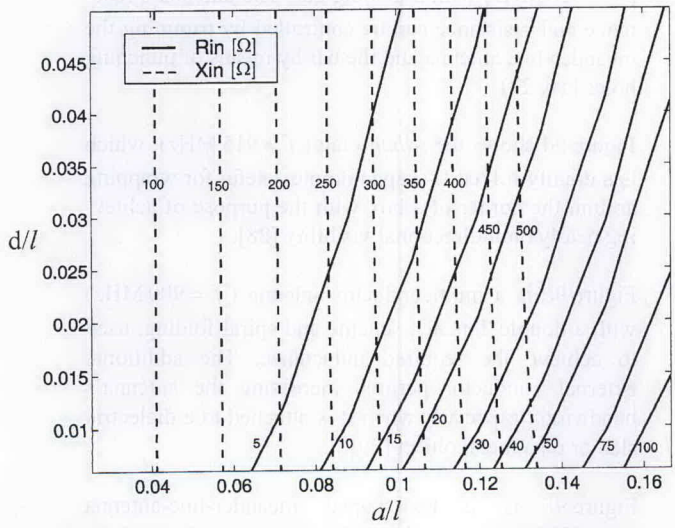

Figure 5. The matching chart for the loop-fed dipole in Figure 4, having fixed $l = \lambda/2$, $w = \lambda/100$, $w' = w/3$, and $a = b$ (square loop).

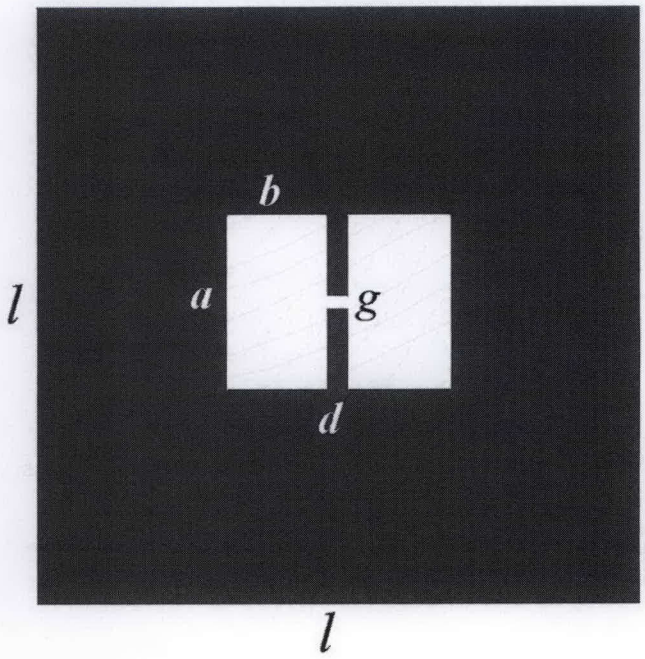

Figure 6a. The geometry of the nested-slot suspended-patch.

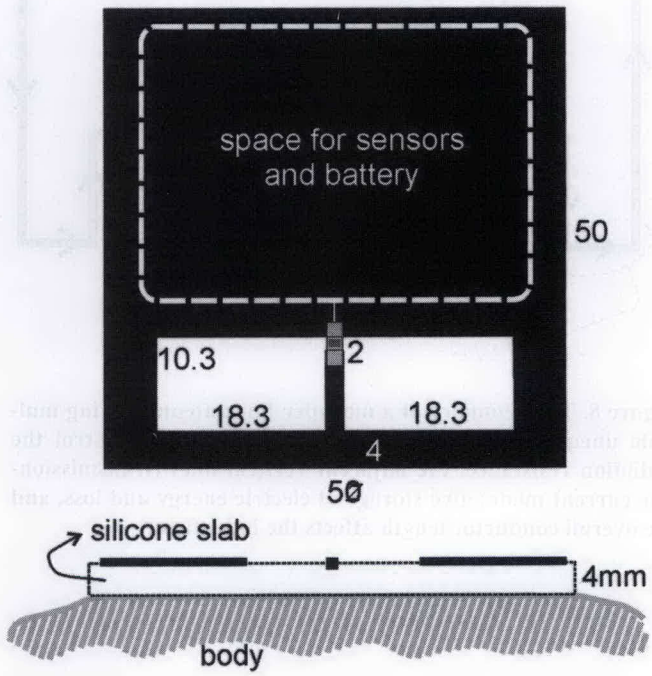

Figure 6b. An example of the tag (size in mm) to be attached onto the human body and able to host sensors [20].

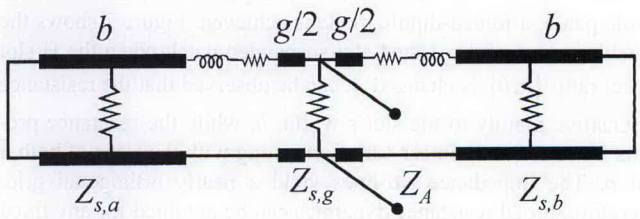

Figure 6c. The equivalent simplified distributed circuit for the tab of Figure 6b.

Authorized licensed use limited to: Intel Corporation via the Intel Library. Downloaded on December 6, 2009 at 18:28 from IEEE Xplore. Restrictions apply.

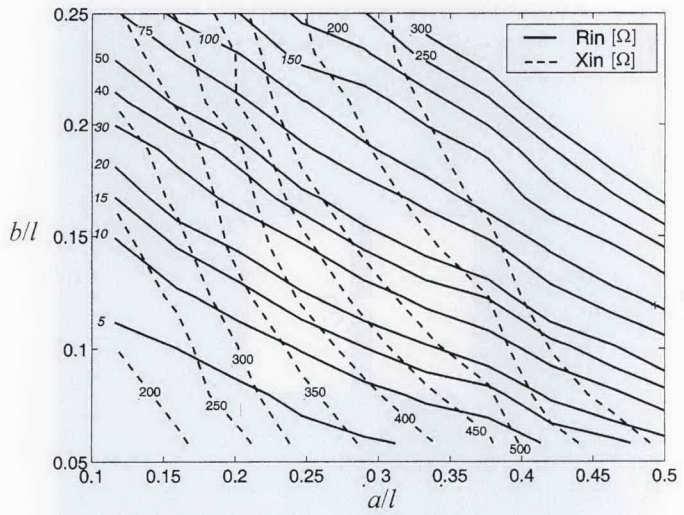

Figure 7. The matching chart for the nested-slot matching layout in Figure 6, for the case of $l = \lambda/2$ and $d = g = \lambda/150$.

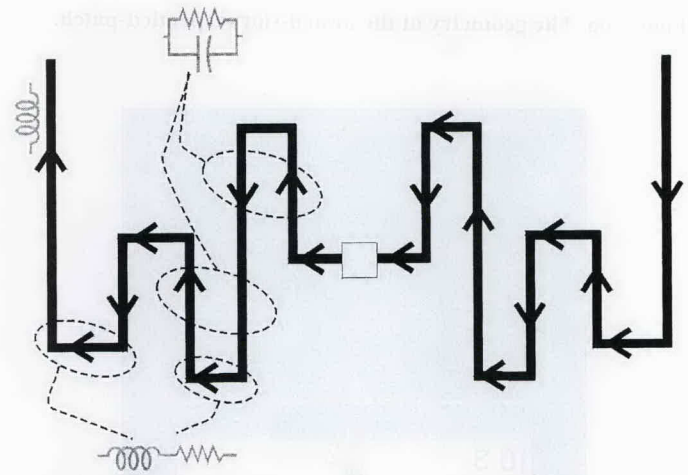

Figure 8. The geometry of a meander-line antenna having multiple unequal turns. The horizontal lines mainly control the radiation resistance, the adjacent vertical lines (transmission-line current mode) give storage of electric energy and loss, and the overall conductor length affects the inductance.

It has been observed [20] that in case where the slot's width is nearly similar to the side of the antenna ($2b \approx l$), the input reactance varies slowly with the frequency, and therefore the tag can remain well tuned within a wide band. When the sizes a and b increase ($2b \approx a \approx l$) until the slot nearly fills the surface of the whole patch, a folded-dipole mode is achieved. Figure 7 shows the matching chart of the nested-slot suspended patch when the H slot aspect ratio $\{a,b\}$ is changed. It can be observed that the resistance is sensitive mainly to the slot's width, b, while the reactance presents fast and nearly linear variations along with the sizes of both a and b. The impedance iso-lines yield a nearly orthogonal grid. Therefore, broad resistance dynamics can be obtained for any fixed reactance value, with a high degree of matching capability.

3. Methods for Size Reduction

Since most UHF RFID tags have to be attached onto small objects, the antenna's geometry needs to be miniaturized without unacceptable degradation of the radiation efficiency. Two size-reduction strategies successfully used to design RFID tags are now reviewed: meandering and inverted-F structures. Both require a single or even multiple folding of the radiating body, but the inverted-F antennas additionally include a finite approximation of a ground plane. Whereas the design of simple tag layouts can be accomplished by using the previously introduced matching charts, geometries with a large number of parameters, such as those described next, often require nondeterministic optimization tools, such as those based on genetic algorithms [23].

3.1 Meandering

As proposed in [24], by folding the arms of a dipole antenna along a meandered path (Figure 8), a wire configuration is produced with distributed capacitive and inductive reactances that globally affect the antenna's input impedance. Up to the first antenna resonance, the currents on the adjacent horizontal segments of meander-line antennas (MLA) have opposite phases. These transmission-line currents do not give a valuable contribution to the radiated power, but nevertheless produce losses. Resonances are achieved at much lower frequencies than in the case of a straight dipole of the same height, at the expense of a narrow bandwidth and a low efficiency.

Figure 9 shows some relevant examples of RFID tag antennas found in recent scientific publications, which use the meander-line technique to reduce the size:

- Figure 9a shows an equi-spaced meander-line antenna ($f = 953$ MHz) with T-match feed [25].
- Figure 9b is a meander-line antenna ($f = 915$ MHz) with an inductively coupled loop feed [26].
- Figure 9c is an equi-spaced meander-line antenna ($f = 920$ MHz) with a loading bar. The antenna's reactance and resistance can be controlled by trimming the meander-line antenna and the bar by means of punching holes [10, 27].
- Figure 9d shows the *Albano* tag ($f = 915$ MHz), which is a doubly-folded L-shaped dipole, useful for wrapping around the corner of a box with the purpose of achieving nearly omnidirectional visibility [28].
- Figure 9e is a multiconductor antenna ($f = 900$ MHz) with a double T-match scheme and spiral folding, used to achieve the required inductance. The additional external conductor permits increasing the antenna's bandwidth, especially when it is attached to a dielectric slab or on a metal object [29].
- Figure 9f is a text-shaped meander-line-antenna ($f = 870$ MHz) tag where the turns are obtained by joining the adjacent letters of the text [30].

Authorized licensed use limited to: Intel Corporation via the Intel Library. Downloaded on December 6, 2009 at 18:28 from IEEE Xplore. Restrictions apply.

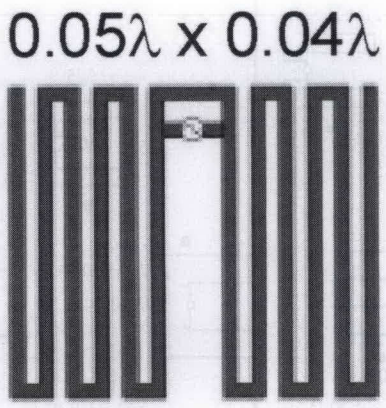

Figure 9a. An equi-spaced meander-line antenna.

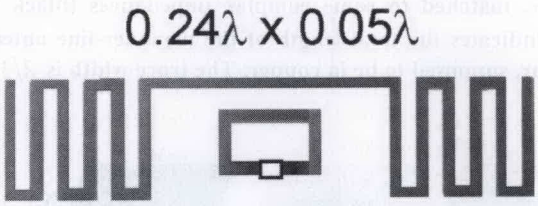

Figure 9b. A meander-line antenna with an inductively coupled loop feed.

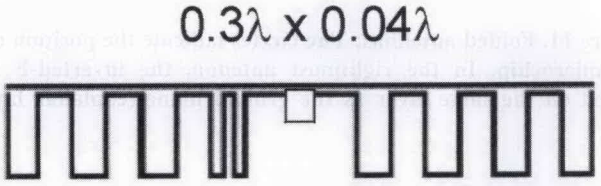

Figure 9c. An equi-spaced meander-line antenna with a loading bar.

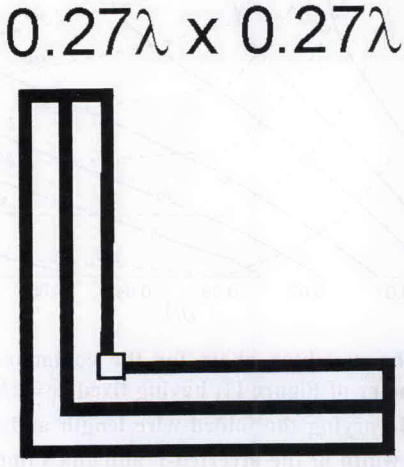

Figure 9d. A doubly-folded L-shaped dipole.

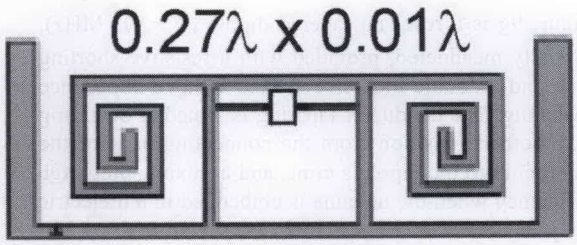

Figure 9e. A multiconductor antenna with a double T-match scheme and spiral folding.

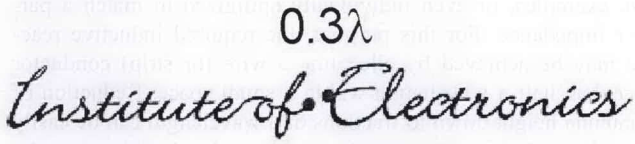

Figure 9f. A text-shaped meander-line antenna.

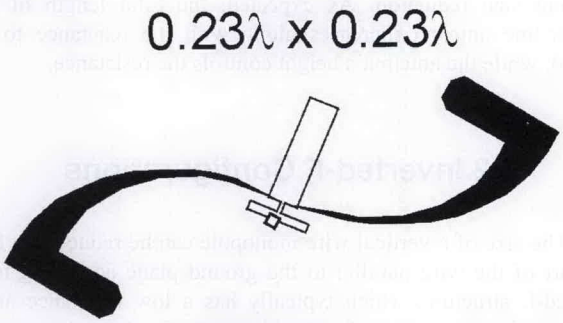

Figure 9g. A resonant tapered dipole that is partially meandered, with a resistive shorting stub and a double inductive stub.

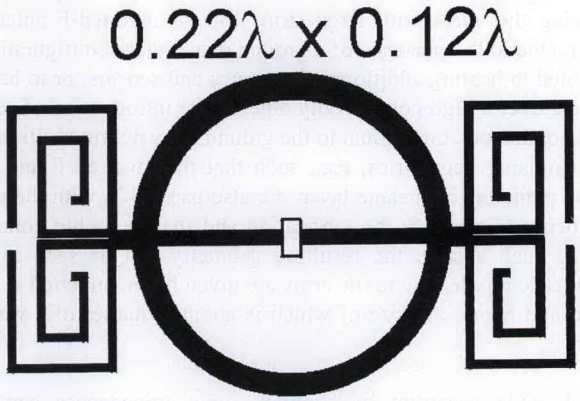

Figure 9h. A multiconductor meander-line tag with a circular-shaped double T-match.

Authorized licensed use limited to: Intel Corporation via the Intel Library. Downloaded on December 6, 2009 at 18:28 from IEEE Xplore. Restrictions apply.

- Figure 9g is a resonant tapered dipole ($f = 915$ MHz), partially meandered, provided with a resistive shorting stub and a double inductive stub to achieve impedance matching. The conductor tapering is aimed at obtaining a smoother transition from the connecting pads of the microchip to the dipole's arms, and at maintaining high efficiency when the antenna is embedded in a dielectric [12].

- Figure 9h shows a multiconductor-meander-line tag ($f = 900$ MHz) with circular-shaped double T-match. The particular meander-line antenna layout is such as to put most of the horizontal currents in phase [31].

The shape of the meanders can be periodic, as in most of the above examples, or even individually optimized to match a particular impedance. For this purpose, the required inductive reactance may be achieved by allocating a wire (or strip) conductor longer than half a wavelength within a small space. Reduction of the antenna height down to fractions of a wavelength can be easily achieved, as shown, for example, in Figure 10. In this case, the meander-line shape was chosen by the genetic-algorithm procedure in [24], for the purpose of maximizing the realized gain, τG_{tag}, with the tag's size constrained within a $\lambda/5 \times \lambda/5$ square. Since the linear conductor's length for the optimized meander-line antenna is generally longer that half a wavelength, the tag's maximum gain may be nearly the same of a regular resonant dipole, in spite of the consistent size reduction. As expected, the total length of the meander-line antenna increases along with the reactance to be matched, while the antenna's height controls the resistance.

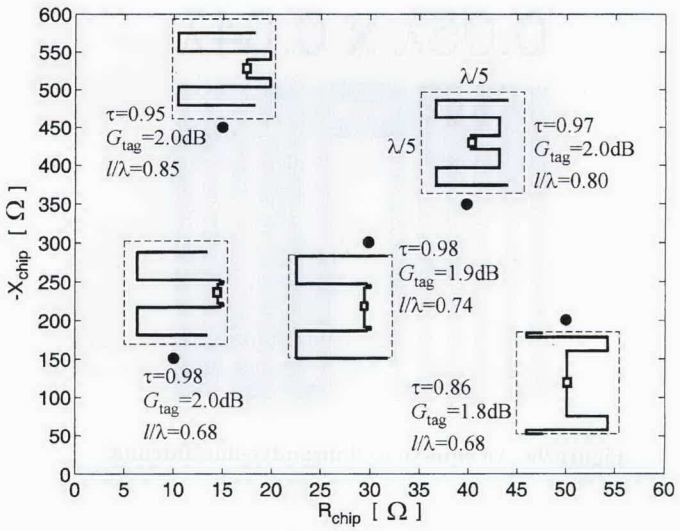

Figure 10. Meander line antennas with a maximum size of $\lambda/5 \times \lambda/5$, matched to some complex impedances (black circles). L indicates the total length of the meander-line antenna conductor, supposed to be in copper. The trace width is $\lambda/300$.

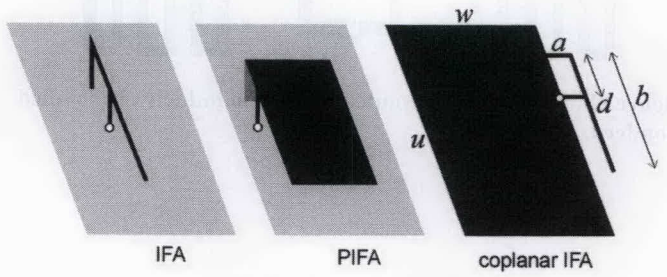

Figure 11. Folded antennas: The circles indicate the position of the microchip. In the rightmost antenna, the inverted-F is placed on the same layer as the ground plane (coplanar layout).

3.2 Inverted-F Configurations

The size of a vertical wire monopole can be reduced by folding part of the wire parallel to the ground plane according to an inverted-L structure, which typically has a low resistance and a high capacitive reactance. To provide tuning freedom, the structure is augmented with a shorting pin, giving the F-type (inverted F antenna, IFA) configuration (Figure 11). This can be also viewed as a monopole version of the T-match, where the radiating body is folded to reduce the space occupied. In the inverted structure, the radiating elements are mainly the conductors orthogonal to the ground plane. The folded conductor, together with its image, yields a transmission-line current mode, producing power loss and only negligible radiation. Therefore, this kind of geometry does not exhibit high efficiency. The antenna bandwidth can be improved by replacing the wires with large strips (planar inverted-F antenna, PIFA). Due to the presence of a ground plane, these configurations are suited to hosting additional electronics and sensors, or to being attached over a high-conductivity object. The introduction of additional conductors, orthogonal to the ground, may permit multi-band tags. Coplanar geometries, e.g., such that the inverted F and the ground plane lay on a same layer, are also used [32], with the purpose being to simplify the fabrication and the microchip connection. In such a case, the resulting geometry can be seen as an asymmetric dipole, where the arms are given by the inverted F and the ground plane, the size of which is about a quarter of a wavelength.

A wide spectrum of complex input impedances can be obtained by varying the geometrical parameters $\{a, b, d\}$. As shown in the matching chart of Figure 12, the input (inductive)

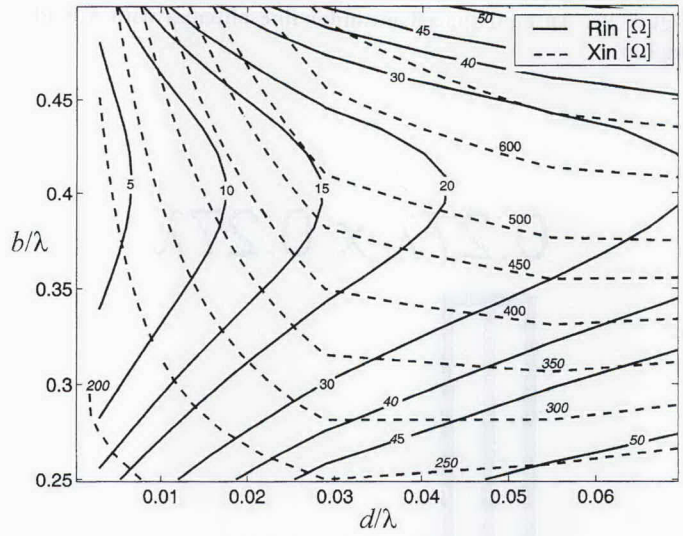

Figure 12. The matching chart for the coplanar inverted-F antenna geometry of Figure 11, having fixed $w = \lambda/4$, $u = \lambda/2$, $a = \lambda/10$, and varying the folded-wire length and the feeding position. The width of the inverted-F antenna's linear conductors was $\lambda/600$.

Authorized licensed use limited to: Intel Corporation via the Intel Library. Downloaded on December 6, 2009 at 18:28 from IEEE Xplore. Restrictions apply.

reactance monotonically increases with both b and d. In contrast, the resistance increases along with d, while it undergoes changes with respect to b around a local minimum value. It could therefore be possible to find two different useful layouts for a given input impedance, having relevant differences in the size b (the length of the conductor parallel to the ground). Finally, the antenna becomes more inductive as the radiating conductor's value of a increases, since the folded part of the antenna moves away from the ground plane. The matching dynamics seems to be comparable to those of the nested-slot suspended-patch configuration.

Some examples of inverted-conductor tags, taken from recent scientific papers, are shown in Figure 13 and summarized in the following.

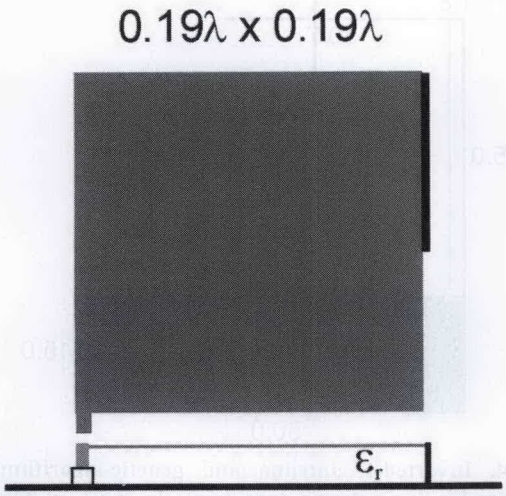

Figure 13a. A conventional two-layer PIFA with a square conductor.

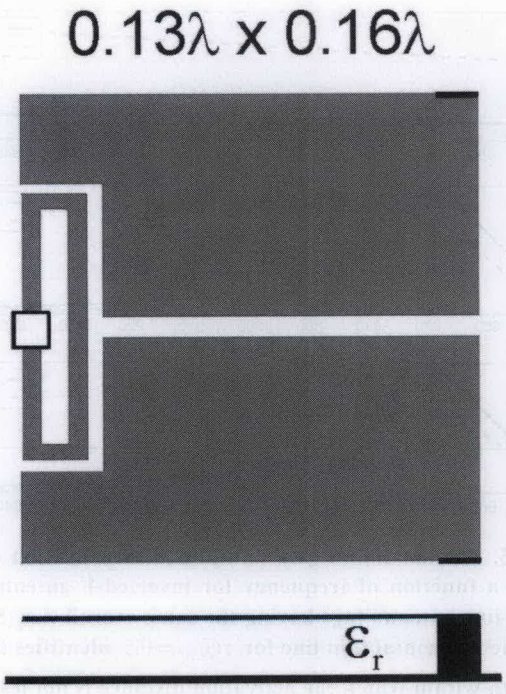

Figure 13b. A two-layer double-PIFA tag with a proximity loop feed.

Figure 13c. A coplanar inverted-F antenna with an additional horizontal stub.

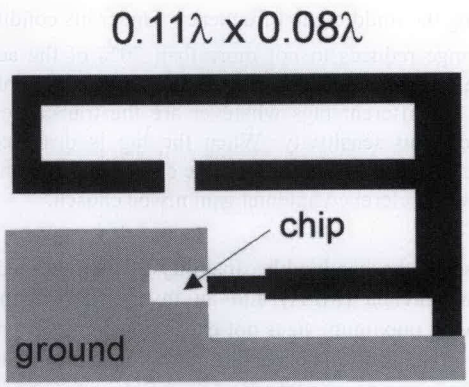

Figure 13d. A coplanar inverted-F antenna with multiple folded conductors to obtain dual-band operation.

- Figure 13a shows a conventional two-layer PIFA ($f = 870$ MHz) with a square conductor. The tag microchip is attached vertically onto the dielectric truncation [33].
- Figure 13b shows a two-layer double-PIFA tag with a proximity loop feed ($f = 900$ MHz). The microchip is placed on the top metallization. The loop is fully integrated within the top conductors [34].
- Figure 13c is a coplanar IFA ($f = 870$ MHz) with an additional horizontal stub [35].
- Figure 13d is a coplanar IFA ($f = 2450$ MHz) with multiple folded conductors to obtain dual-band operation at 2400 MHz and 5300 MHz [36].

Authorized licensed use limited to: Intel Corporation via the Intel Library. Downloaded on December 6, 2009 at 18:28 from IEEE Xplore. Restrictions apply.

3.3 Bandwidth Issues

Unlike conventional 50 Ω-matched antennas, the most useful parameter for the definition of an RFID tag's bandwidth is the realized gain, rather than the return loss, as it is also in the design of ultra-wideband antennas [37]. In fact, the tag's bandwidth depends on the required minimum reading range in the specific application. Once fixed by the power constraints, this can be therefore be related to the system parameter τG_{tag}. Indeed, the stability of the realized gain over the frequency gives the *rangewidth* of the reader-tag system.

In general, it is well known that antenna miniaturization yields layouts with reduced bandwidth. Although RFID applications involve narrow frequency bands, bandwidth issues are nevertheless important. Tag impedance may be easily detuned by coupling with the objects to be tagged, as well as by the interaction with the surrounding environment, and the resulting reading range could be globally degraded.

In order to introduce a general bandwidth definition that is not dependent on the particular application, a perfectly matched isotropic antenna ($\left[\tau G_{tag}\right]_0 = 1$) is selected as a reference. The tag's band is then defined as the frequency range, $[f_{min}, f_{max}]$, where the following condition holds:

$$\left[\tau G_{tag}\right](f) = \frac{1}{2}\left[\tau G_{tag}\right]_0(f_c), \qquad (6)$$

with f_c being the middle-band frequency. Under his condition, the activation range reduces to not more than 70% of the activation range of the reference antenna. This definition permits comparing the features of different tags whatever are the transmitter power and the microchip sensitivity. When the tag is designed to be attached over a high-loss target, as in the case of the human body, a different (lower) reference-antenna gain my be chosen.

To discuss the bandwidth capability of miniaturized tags, a meander-line antenna (MLA) and an inverted-F antenna (IFA) antenna, having maximum sizes not exceeding 5 cm × 5 cm (about $\lambda/7$ at 870 MHz), and matched to a high-impedance-phase-angle microchip ($Z_{chip} = 15 - j450\,\Omega$), are now analyzed with respect to frequency changes. With reference to Figure 14, the inverted-F antenna's vertical conductors occupy most of the available space with the purpose of achieving the required input resistance. The meander-line antenna was automatically optimized as previously discussed. In particular, under only the constraint of best realized gain, the solution found by the genetic optimizer was slightly smaller than the imposed maximum size. No bandwidth constraint was considered.

Figure 15 shows the tags' features (maximum gain, power-transmission factor, and realized gain) with respect to the variation in frequency. The meander-line antenna exhibited a gain larger than the inverted-F antenna's gain. Nevertheless, the gain was only slightly frequency dependent, and the bandwidth performance was therefore manly affected by the impedance matching. The meander-line antenna geometry permitted a better realized gain ($\tau G_{tag} = 1.46$) at 870 MHz than the inverted-F antenna design ($\tau G_{tag} = 1.33$), but the activation range improvement at that frequency was only about 5%.

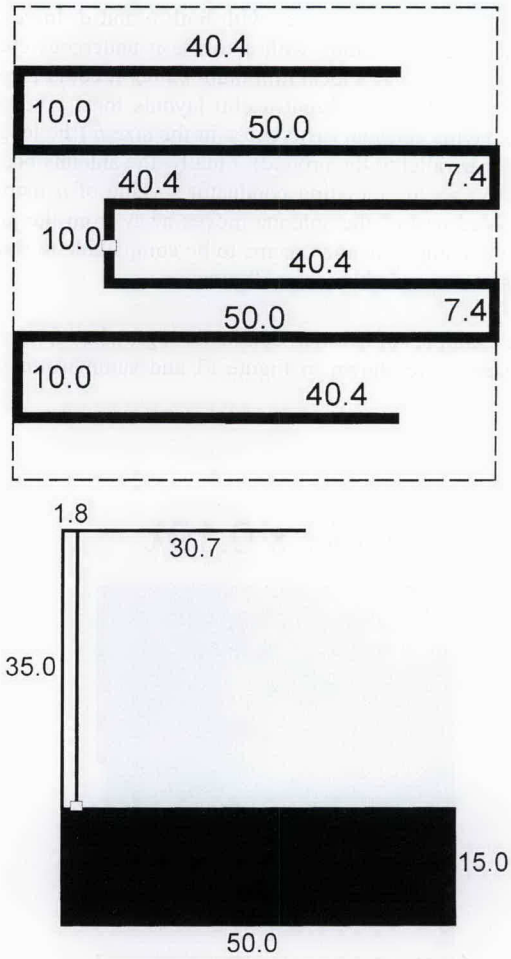

Figure 14. Inverted-F antenna and genetic-algorithm-optimized meander-line-antenna tags (sizes in mm), matched at 870 MHz to the microchip impedance $Z_{chip} = 15 - j450\,\Omega$. The maximum external sizes are 5 cm × 5 cm ($\approx 0.14\lambda$). The trace size is 1 mm.

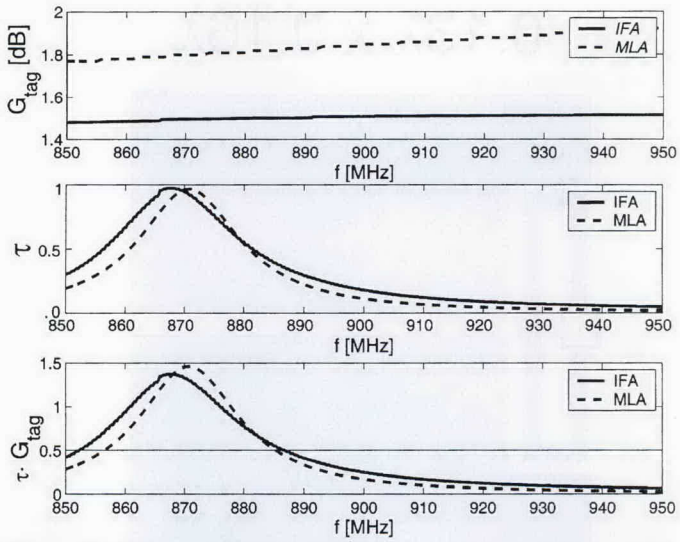

Figure 15. The maximum gain and power transmission coefficients as a function of frequency for inverted-F antenna and meander-line antenna tags having the same overall size (5 cm × 5 cm). The horizontal thin line for $\tau G_{tag} = 0.5$ identifies the tag bandwidth within which the activation distance is not less than 70% of the activation distance of a reference perfectly matched isotropic antenna.

Authorized licensed use limited to: Intel Corporation via the Intel Library. Downloaded on December 6, 2009 at 18:28 from IEEE Xplore. Restrictions apply.

Table 1. The bandwidth features of the 870 MHz meander-line-antenna (MLA) and inverted-F-antenna (IFA) tags having the same maximum external size of 5 cm × 5 cm.

	MLA	IFA
f_{min}	856 MHz	852 MHz
f_{max}	885 MHz	887 MHz
Δf	29 MHz	35 MHz
B	3.3%	4.0%

According to the above definition, the bandwidth features of the examples considered are reported in Table 1, where $\Delta f = f_{max} - f_{min}$ and $B = \Delta f / f_c$. Although the two antennas showed a nearly similar narrow bandwidth, as expected by the relevant size reduction, the inverted-F antenna's layout had a slightly broader relative bandwidth. However, it must also be considered that the meander-line antenna layout possesses a larger number of degrees of freedom compared to the standard inverted-F antenna. Additional constraints may therefore be included in the meander-line-antenna optimization procedure for the purpose of bandwidth enhancement.

4. Other Designs (Dual-Band, Dual-Polarization, and Near-Field Tags)

Some issues concerning the design of particular tags that are not fully included in the previous classification – such as dual-band and dual-polarized tags, and the new near-field UHF tags – are now briefly discussed.

4.1 Dual-Band Tags

Multi-band operation is traditionally achieved in antennas by using several resonant elements or by exploiting high-order harmonics. Some dual-band design solutions have been recently proposed to achieve 870 MHz and 2.45 GHz or 2.45 GHz and 5.8 GHz compact multifunction transponders. The basic idea is to load a traditional tag antenna with parasitic tuning elements, such as inner slots or a tuning stub. The goal is to avoid a size increase, and the tuning elements are engineered to be embedded inside the radiating element, itself. Figure 16 shows four examples of dual-band tags.

Figure 16a shows a planar antenna [38] with shaped slots, used to both achieve two working frequencies (resonances or complex impedance matching) at 868 MHz and 2450 MHz, and to reduce the antenna's size at the smaller frequency. Figure 16b is a microstrip Sierpinsky gasket printed antenna [39], optimized for dual-band operation at 2.45 GHz and 5.8 GHz. A microstrip line feeds the first iteration of the Sierpinsky fractal metallization, and the ground plane under the radiating element is removed. The metallic triangle's size fixes the fundamental mode, while the inner triangular slot determines the second resonance.

A slot-loaded dipole [40] for operation at 870 MHz and 2450 MHz is shown in Figure 16c. A coupled slot is introduced here within the dipole's conductor, the global length of which fixes the lower working frequency. The slot acts as a sort of current trap

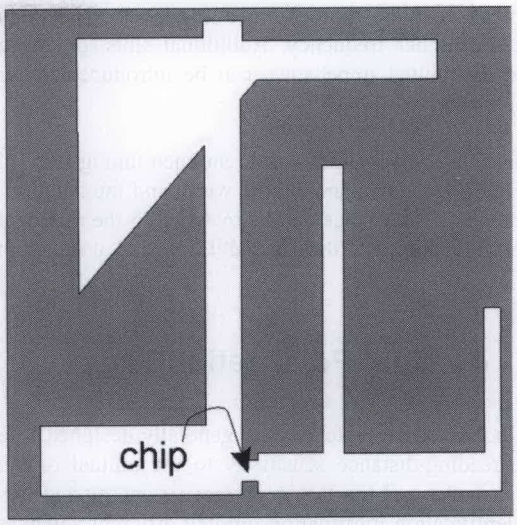

Figure 16a. A planar antenna with shaped slots for a dual-band tag.

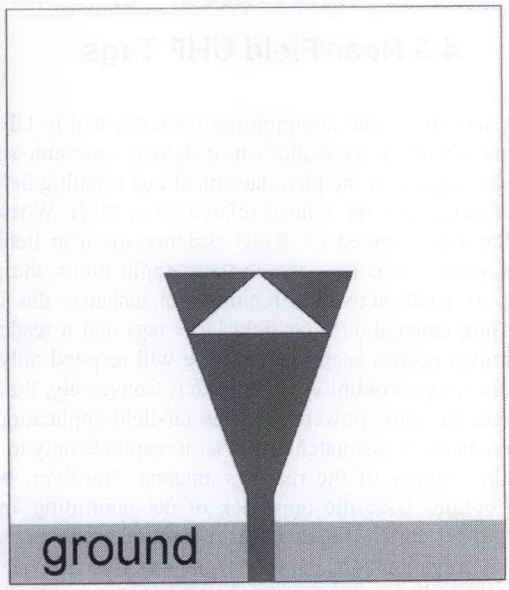

Figure 16b. A microstrip Sierpinsky gasket printed antenna for dual-band operation.

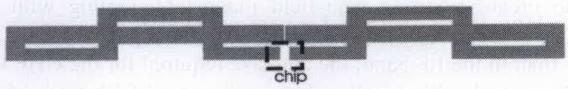

Figure 16c. A slot-loaded dipole for dual-band operation.

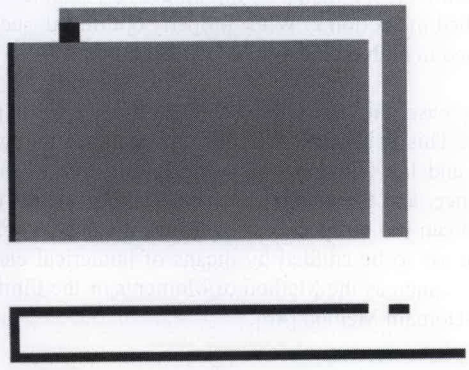

Figure 16d. A dual-band planar inverted-F antenna.

Authorized licensed use limited to: Intel Corporation via the Intel Library. Downloaded on December 6, 2009 at 18:28 from IEEE Xplore. Restrictions apply.

[41] that breaks off the dipole into a smaller-length conductor working at the higher frequency. Additional slots, or any other lumped and distributed impedance, can be introduced to further tune the impedance.

A planar inverted-F antenna with an open tuning stub [42] is shown in Figure 16d. By changing the width and the length of the stub, the antenna's impedance can be matched to the microchip at two different frequencies (870 MHz and 915 MHZ) at same time.

4.2 Dual-Polarization Tags

Dual-polarized tag antennas are generally designed to either reduce the reading-distance sensitivity to the mutual orientation between the reader and the tag, or to receive energy and transmit back the identification information through different antennas and polarizations. In these designs, orthogonal slots [43], driving a conventional patch tag, or crossed dipoles [44], can be used.

4.3 Near-Field UHF Tags

Very recently, some attention has been devoted to UHF tags that are able to work in the reader's near field as a possible solution to item-level tagging in the pharmaceutical and retailing industries (see the overview and the related references in [45]). When compared to the well-assessed LF RFID systems, the near-field UHF tags could promise smaller sizes. In these applications, the goal is to create very small activation regions. For instance, this can be done by using conventional far-field UHF tags and a reader with low transmitted power, such that each tag will respond only when placed in the close proximity of the reader. Conversely, the reader could radiate the same power, as in the far-field applications, but the tag impedance is mismatched so that it responds only to strong fields in the vicinity of the reader's antenna. However, both of these two options have the drawback of not permitting any size reduction of the tag (in the first case), and of producing a non-localized interrogation zone (in the second case), so that the reader may unintentionally see some other long-range tags present in the far-field region.

More-efficient tag design consists of introducing a coil element to create a strong near-field magnetic coupling with the reader, as in the case of LF systems. Due to the higher working frequency than in the LF band, the coil size required for the UHF tags could be considerably smaller than in the case of LF tags. Moreover, such a coil could be also integrated with a dipole-like antenna, such as the T-match or the inductively coupled loop layouts described in Section 2. When properly optimized, such layouts could be used in both the near- and far-field regions.

In any case, the design of near-field UHF tags has particular complexity. This is because the electromagnetic coupling between the reader and the tag may not be neglected, due to the mutual small distance, and the antenna performance parameters (gain and impedance) can not be specified independently. The whole system therefore needs to be studied by means of numerical electromagnetic solvers, such as the Method of Moments or the Finite-Difference Time-Domain Method [46].

5. Tag Measurement and Testing

The measurement of tag performance is a not-yet-assessed issue, in contrast to the case of more-conventional 50-Ω-matched antennas. The tag is in fact designed to work as a back-scattering antenna, and it is connected to the microchip, which is a nonlinear load. Three different measurement strategies are typically adopted: i) measurement of the chip-less tag's input impedance and gain, ii) measurement of the tag's radar cross section for different loading impedances, and iii) measurement of the reading distance when a reader-tag link is established. In all of the cases, since the tag is designed to be attached onto a class of targets, a reference object should be included in the measurement in order to have reliable data.

5. 1 Measurement of Input Impedance and Gain

This is the most general measurement of the specific tag performance. The critical issue is the connection of the vector network analyzer's (VNA's) probe to the tag's terminals, in the absence of the microchip. Since the tag is not designed as a transmitting antenna, a balanced connection of the vector network analyzer's coaxial cable to the tag's port often requires a balun or a choke. In this case, particular care has to be devoted to avoid impedance and pattern distortion. Accurate measurement schemes can be achieved in the case where the tag is a grounded antenna, as in some of the (planar) inverted-F-antenna-like structures previously described, or when the tag possesses an electric symmetry plane. Under this last condition, only half of the antenna needs to be fabricated, and the vector network analyzer's probe can be placed in the ground plane's side that is opposite to the antenna half-space. For instance, Figure 17 shows the measurement setup [21] of the nested-slot

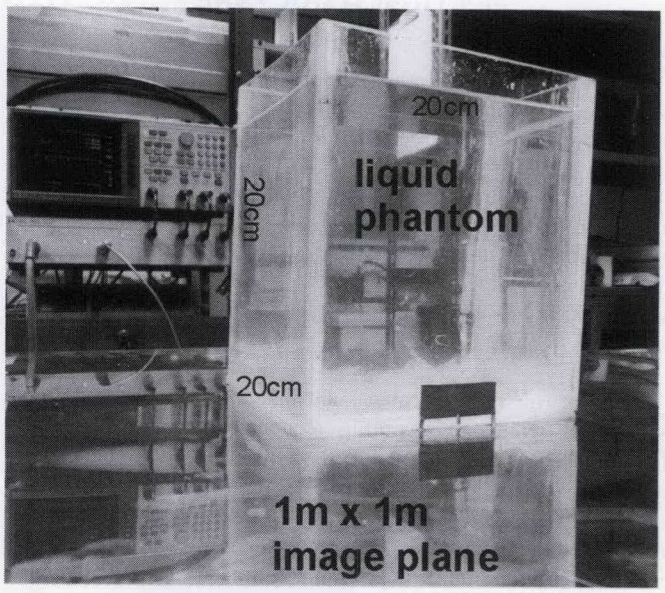

Figure 17. A copper prototype of a nested-slot suspended-patch antenna (NSSP) antenna designed for a muscle-like box. A coaxial (SMA) connector is on the reverse side of the image plane.

Authorized licensed use limited to: Intel Corporation via the Intel Library. Downloaded on December 6, 2009 at 18:28 from IEEE Xplore. Restrictions apply.

suspended-patch antenna reviewed in Figure 6. The antenna's gain can be measured by standard techniques, and all the tag's performance indicators (realized gain, bandwidth, reading distance) can be then calculated in post processing, and are scenario and reader independent.

5.2 Measurement of the Tag's Radar Cross Section

A relevant part of reader-tag communication consists of the tag's backscattering of the continuous wave coming from the reader. During this task, the microchip acts as a programmable switching device, which connects or disconnects the antenna to a Z_{mod} load (typically, an open circuit or a high impedance for the low state, and a short circuit or the antenna's conjugate impedance for the high state). During the data transfer, the RFID system can be considered to be a monostatic radar, and it therefore can be characterized by the radar cross section (RCS), σ_T. As discussed in detail and experimentally verified in [47], the RCS of many classes of tag antennas can be easily related to the antenna's gain and input impedance by

$$\sigma_T = \frac{\lambda^2 G^2 R_A}{\pi |Z_A + Z_{mod}|^2}. \qquad (6)$$

The RCS of the chip-less tag can be then measured as the S_{11} variation at the port of an illuminating antenna, in both an anechoic chamber or a real scenario. The measurements are generally repeated for different impedances Z_{mod}. Although this is an indirect measurement that does not give any direct information about the input impedance and the activation range, it is nevertheless a reader-independent characterization.

5.3 Measurement of the Reading Distance

This is an application- and scenario-specific measurement since besides the choice of the target, it is strictly related to the features of the reader and to the transmitting power. It requires that a particular microchip be physically connected at the tag antenna's port [48]. Measurements can be also performed in a controlled environment, such as an anechoic camber or a TEM cell, as described in detail in [10]. Typical diagrams of the reading range as a function of distance and reader power are generally produced. This measurement is the simplest to perform. In the case of real scenarios, it does not require any particular or expensive equipment besides a reader, and provides a true system performance evaluation. However, the features of the tag itself are hidden within the overall results. This procedure is therefore of less general meaning than the previous measurement schemes.

6. Concluding Remarks

Several basic design layouts have been discussed. The meander-line antenna configurations exhibit the largest number of degrees of freedom, which can be globally optimized to suit the tag to a large variety of microchips and sizes. The tagged object can also be accounted for in the antenna design procedure by employing layered media models. The (planar) inverted-F antenna structures are instead particularly attractive for metallic objects. In addition to the (planar) inverted-F antenna, the nested-slot suspended-patch antenna can be useful for hosting sensors and electronics.

The available know-how, scattered all over the open technical literature, seems to be mature and rich enough for approaching the design of conventional UHF passive RFID tags. However, due to the general requirements of small size, the resulting antenna bandwidth is narrow, no matter which configuration is chosen. The antenna's performance is therefore strongly dependent on the nearby environment. The open challenge is therefore the design of antennas the input and radiation properties of which remain nearly unchanged when the tag is attached to different substrates, such as paper, wood, metal, or living tissues. The problem is particularly hard in the presence of metals, and the (planar) inverted-F-antenna-like structures give only a partial solution.

Further research efforts could be devoted to the design methodology of RFID tag antennas for sensor networks, where the tag should by tightly integrated with the sensor and electronics.

7. Acknowledgments

The author wishes to thank Claudio Calabrese for his enthusiastic and valuable support in documentation and computer simulations.

8. References

1. H. Stockman "Communication by Means of Reflected Power," *Proceedings of the IRE*, **36**, 10, October 1948, pp. 1196-1204.

2. J. Landt, "The History of RFID," *IEEE Potentials*, **24**, 4, October-November 2005, pp. 8-11.

3. A. R. Koelle, S. W. Depp, and R. W. Freyman, "Short-Range Radio-Telemetry for Electronic Identification, Using Modulated RE Backscatter," *Proceedings of the IEEE*, **63**, 8, August 1975, pp. 1260-1261.

4. A. R. Koelle, "Short Range UHF Telemetry System Using Passive Transponders for Vehicle ID and Status Information," *IEEE Workshop on Automotive Applications of Electronics*, Dearborn MI, October 1988, pp. 34-38.

5. K. Finkenzeller, *RFID Handbook*, New York, Wiley & Son, 2000.

6. R. Want, "An Introduction to RFID Technology," *IEEE Pervasive Computing*, **5**, 1, January-March 2006, pp. 25-33.

7. R. Bansal, "Coming Soon to a Wal-Mart Near You," *IEEE Antennas Propagation. Magazine*, **45**, 6, December 2003, pp. 105-106.

8. S. Nambi, S. Nyalamadugu, S. M. Wentworth and B. A. Chin, "Radio Frequency Identification Sensors," *Proc. 7th World Multiconf. Systemics, Cybernetics & Informatics (SCI 2003)*, Orlando, FL, June 2003, pp. 386-390.

Authorized licensed use limited to: Intel Corporation via the Intel Library. Downloaded on December 6, 2009 at 18:28 from IEEE Xplore. Restrictions apply.

9. R. S. Sangwan, R. G. Qiu and D. Jessen "Using RFID Tags for Tracking Patients, Charts and Medical Equipment within an Integrated Health Delivery Network," *IEEE Int. Conf. Networking Sensing and Control*, 2005, pp. 1070-1074.

10. K. V. S. Rao, P. V Nikitin and S. F. Lam, "Antenna Design for UHF RFID Tags: A Review and a Practical Application," *IEEE Transactions on Antennas and Propagation*, **AP-53**, 12, December 2005, pp. 3870-3876.

11. J. Curty, N. Joehl, C. Dehollain and M. J. Delercq, "Remotely Powered Addressable UHF RFID Integrated System," *IEEE Journal of Solid-State Circuits*, **40**,11, November 2005, pp. 2193-2202.

12. S. Basat, S. Bhattacharya, A. Rida, S. Johnston, L. Yang, M. M. Tentzeris and J. Laskar , "Fabrication and Assembly of a Novel High-Efficiency UHF RFID Tag on Flexible LCP Substrate," *Electronic Components and Technology Conference*, May-June 2006, pp. 1352-1355.

13. H. W. Son, J. Yeo, G. Y. Choi, and C. S. Pyo, "A Low-Cost, Wideband Antenna for Passive RFID Tags Mountable on Metallic Surfaces," IEEE International Symposium on Antennas and Propagation *Digest*, Albuquerque, NM, June 2006, pp. 1019-1022.

14. S. Uda and Y. Mushiake, *Yagi-Uda Antenna*, Tokyo, Sasaki Printing and Publishing Co., 1954, pp. 119-131.

15. C. A. Balanis, *Antenna Theory, Analysis and Design, Second Edition*, New York, John Wiley & Sons Inc., 1997.

16. L. Ukkonen, M. Schaffrath, J. A. Kataja, L. Sydanheimo and M. Kivikoski, Evolutionary RFID Tag Antenna Design for Paper Industry Applications, *International Journal of Radio Frequency Identification Technology and Applications*, **1**, 1, January 2006, pp. 107-122.

17. H. W. Son and C. S. Tyo, "Design of RFID Tag Antennas Using an Inductively Coupled Feed," *Electronics Letters*, **41**, 18, September 2005, pp. 994-996.

18. Y. Lee, "Antenna Circuit Design for RFID Applications," Microchip Technology Inc., Application Note AP710, 2003, available at http://ww1.microchip.com/downloads/en/AppNotes/00710c.pdf.

19. EM Software & Systems-S.A. (Pty) Ltd., *FEKO User's Manual, Suite 5.1*, Stellenbosch, South Africa, December 2005, available at http://www.feko.info.

20. G. Marrocco, "Body-Matched Antennas for Wireless Biometry," *European Conference on Antennas and Propagation*, Nice, France, November 2006, p. 795.

21. G. Marrocco, "RFID Antennas for the UHF Remote Monitoring of Human Subjects," *IEEE Transactions on Antennas and Propagation*, **AP-55**, 6, June 2007, pp. 1862-1870.

22. G. Marrocco and C. Calabrese, "Automatic Design of Miniaturized Slot-Line RFID Antennas," Second European Conference on Antennas and Propagation (EUCAP), Edinburgh, Scotland, November 2007.

23. D. S. Weile and E. Michielsen, "Genetic Algorithm Optimization Applied to Electromagnetics: A Review," *IEEE Transactions on Antennas and Propagation*, **AP-45**, 3, March 1997, pp. 343-353.

24. G. Marrocco, "Gain-Optimized Self-Resonant Meander Line Antennas for RFID Applications," *IEEE Antennas and Wireless Propagation Letters*, **2**, 2003, pp. 302-305.

25. N. Michishita and Y. Yamada, "A Novel Impedance Matching Structure for a Dielectric Loaded 0.05 Wavelength Small Meander Line Antenna," *IEEE International Symposium on Antennas and Propagation*, Albuquerque, NM, July 2006, pp. 1347-1350.

26. W. Choi, H. W. Son, C. Shin, J.-H. Bae and G. Choi, "RFID Tag Antenna with a Meandered Dipole and Inductively Coupled Feed," *IEEE International Symposium on Antennas and Propagation*, Albuquerque, NM, July 2006, pp. 619-622.

27. A. Toccafondi and P. Braconi, "Compact Load-Bars Meander Line Antenna for UHF RFID Transponder," *European Conference on Antennas and Propagation*, Nice, France, November 2006, p. 804.

28. S. A. Delichatsios, D. W. Engels, L. Ukkonen and L. Sydänheimo, "Albano Multidimensional UHF Passive RFID Tag Antenna Designs," *Int. J. Radio Frequency Identification Technology and Applications*, **1**, 1, January 2006, pp. 24-40.

29. C. Cho, H. Choo and I. Park, "Design of Novel RFID Tag Antennas for Metallic Objects," IEEE International Symposium on Antennas and Propagation *Digest*, Albuquerque, NM, July 2006, pp. 3245-3248.

30. M. Keskilammi and M. Kivikoski, "Using Text as a Meander Line for RFID Transponder Antennas," *IEEE Antennas and Wireless Propagation Letters*, **3**, 2004, pp. 372-374.

31. Y. Tikhov, Y. Kim and Y.-H. Min, "Compact Low Cost Antenna for Passive RFID Transponder," IEEE International Symposium on Antennas and Propagation *Digest*, Albuquerque, NM, July 2006, pp. 1015-1018.

32. C. Soras, M. Karaboikis, G. Tsachtsiris and V Makios, "Analysis and Design of an Inverted-F Antenna Printed on a PCMCIA Card for the 2.4 GHz ISM Band," *IEEE Antennas and Propagation Magazine*, **44**, 1, February 2002, pp. 37-44.

33. H. Hirvonenen, P. Pursula, K. Jaakkola and K. Laukkanen, "Planar Inverted-F Antenna for Radio Frequency Identification," *Electronics Letters*, **40**, 14, July 2004, pp. 848-850.

34. B. Yu, S.-J. Kim, B. Jung, F. J. Harackiewicz, M.-J. Park and B. Lee, "Balanced RFID Tag Antenna Mountable on Metallic Plates," IEEE International Symposium on Antennas and Propagation *Digest*, Albuquerque, NM, July 2006, pp. 3237-3240.

35. C. H. Cheng and R. D. Murch, "Asymmetric RFID Tag Antenna," IEEE International Symposium on Antennas and Propagation *Digest*, Albuquerque, NM, July 2006, pp. 1363-1366.

36. I. Y. Chen, C. U. Huang, H. H. J. Chen, C. F. Jou and S. R. S. Huang, "Folded Dual-Band (2.4/5.2 GHz) Antenna Fabricated on Silicon Suspended Parylene Membrane," *Asia Pacific Microwave Conference Proceedings*, December 2005, 4, pp. 4-8.

Authorized licensed use limited to: Intel Corporation via the Intel Library. Downloaded on December 6, 2009 at 18:28 from IEEE Xplore. Restrictions apply.

37. X. H. Wu and Z. N. Chen, "Comparison of Planar Dipoles in UWB Applications," *IEEE Transactions on Antennas and Propagation*, **AP-53**, 6, June 2005, pp. 1973-1983.

38. C. Diugwu and J. C. Batchelor, "Analysis of the Surface Distribution in a Dual Band Planar Antenna for Passive RFID Tag," IEEE International Symposium on Antennas and Propagation *Digest*, Washington, NY, July 2005, pp. 459-462.

39. S. Tedjini, T. Voung, and V. Beroulle, "Antennas for RFID Tags," *Joint sOc-EUSAI Conference*, Grenoble, France, 2005, pp. 19-22.

40. S. Jeon, Y. Yu, S. Kahng, J. Park, N. Kim and J. Choi, "Dual-Band Dipole Antenna for ISO 18000-6/ISO 18000-4 Passive RFID Tag Applications," IEEE International Symposium on Antennas and Propagation *Digest*, Albuquerque, NM, July 2006, pp. 4285-4288.

41. L. Mattioni and G. Marrocco, "BLADE: A Broadband Loaded Antennas DEsigner," *IEEE Antennas and Propagation Magazine*, **48**, 5, October 2006, pp.120-129.

42. M. Hirvonen, K. Jaakkola, P. Pursula and J. Saily, "Dual-Band Platform Tolerant Antennas for Radio-Frequency Identification," *IEEE Transactions on Antennas and Propagation*, **AP-54**, 9, September 2006, pp. 2632-2636.

43. S. Nambi and S. M. Wenthworth, "5.8 GHz Dual-Polarized Aperture-Coupled Microstrip Antenna," IEEE International Symposium on Antennas and Propagation *Digest*, Washington, DC, July 2005, pp. 235-238.

44. M. Stupf, R. Mittra, J. Yeo and J. R. Mosig, "Some Novel Design for RFID Antennas and their Performance Enhancement with Metamaterials," IEEE International Symposium on Antennas and Propagation *Digest*, Albuquerque, NM, July 2006, pp. 1023-1026.

45. P. V. Nikitin, K.V. Rao and S. Lazar, "An Overview of Near Field UHF RFID," *IEEE Int. Conf. on RFID*, March 2007, pp. 167-173.

46. A. Taflove, *Computational Electromagnetics: The Finite Difference Method*, Norwood, MA, Artech House, 1995.

47. P. Nikitin and K. V. S. Rao, "Theory and Measurement of Backscattering from RFID Tags," *IEEE Antennas and Propagation Magazine*, **48**, 6, December 2006, pp. 212-218.

48. L. Ukkonen, L. Sydänheimo and M. Kivikoski "Effects of Metallic Plate Size on the Performance of Microstrip Patch-Type Tag Antennas for Passive RFID," *IEEE Antennas and Wireless Propagation Letters*, **4**, 2005, pp. 410-413.

Introducing the Feature Article Author

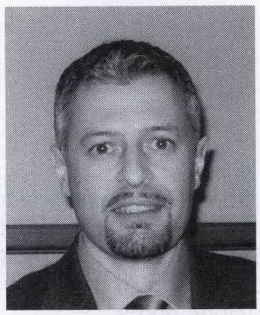

Gaetano Marrocco received the Laurea in Electronic Engineering and the PhD in Applied Electromagnetics from the University of L'Aquila, Italy, in 1994 and 1998, respectively. Since 1997, he has been a Researcher at the University of Rome "Tor Vergata," Rome, Italy, where he currently teaches "Antenna Design" and "Bioelectromagnetics." In the summer of 1994, he was at the University of Illinois at Urbana-Champaign as a postgraduate student. In autumn 1999, he was a visiting researcher at the Imperial College in London, UK. His research is mainly directed toward the modeling and design of broadband and ultra-wideband antennas and arrays, as well as toward miniaturized antennas for RFID applications. He has been involved in several space, avionic, naval, and vehicular programs of the European Space Agency, NATO, Italian Space Agency, and the Italian Navy. He holds two patents on broadband naval antennas, and one patent on sensor RFID systems. He currently serves as Associate Editor of the *IEEE Wireless and Guided Wave Letters*.

Authorized licensed use limited to: Intel Corporation via the Intel Library. Downloaded on December 6, 2009 at 18:28 from IEEE Xplore. Restrictions apply.